Frontiers of Physics
https://doi.org/10.1007/s11467-018-0862-3
Front. Phys.
14(1), 13502 (2019)

LETTER

# Tuning spin reorientation in $Er_{1-x}Y_xFeO_3$ single crystal family

**Ning Yuan[1], Ru-Bin Li[1], You-Shuang Yu[1], Zheng-Jie Feng[2], Bao-Juan Kang[1], Shi-Yi Zhuo[3], Jun-Yi Ge[2], Jin-Cang Zhang[2], Shi-Xun Cao[1,2,†]**

[1] *Department of Physics, International Center of Quantum and Molecular Structures, Shanghai University, Shanghai 200444, China*
[2] *Materials Genome Institute, Shanghai University, Shanghai 200444, China*
[3] *Shanghai Institute of Ceramics, Chinese Academy of Sciences, Shanghai 200050, China*
*Corresponding author. E-mail:* [†] *sxcao@shu.edu.cn*
*Received July 6, 2018; accepted August 24, 2018*

A temperature-induced spin reorientation transition between $\Gamma_4$ ($G_x$, $A_y$, $F_z$) and $\Gamma_2$ ($F_x$, $C_y$, $G_z$) has been studied in the family of $Er_{1-x}Y_xFeO_3$ ($x = 0$, 0.25, 0.5, 0.75, 1) single crystals. By doping nonmagnetic $Y^{3+}$, we tuned the spin reorientation temperature to low temperature with increasing $x$. Moreover, the typical compensation point and spin flip transition of $ErFeO_3$ also decreases with doping, and disappears above $x = 0.75$. We also report the Rietveld refinements and Raman spectroscopy of $Er_{1-x}Y_xFeO_3$, where some Raman peaks are shifted to low frequency with increasing doping. Our results shed light on the understanding of the interaction between two magnetic sub-lattices of rare earth ($R^{3+}$) and iron ($Fe^{3+}$) ions, and will also contribute to the materials design and potential applications.

**Keywords** $Er_{1-x}Y_xFeO_3$, single crystal growth, magnetic measurements

## 1 Introduction

Rare-earth orthoferrites $RFeO_3$ ($R$ = rare-earth ions and Y) have a distorted perovskite structure with a space group of *Pbnm*. Owing to the distorted structure and the presence of Dzyaloshinskii–Moriya interaction, they exhibit an antiferromagnetic structure, and is therefore widely used in many research areas [1]. Spin reorientation transition (SRT) is a widely studied content for $RFeO_3$, and White *et al.* had reported the mechanism of this transition in detail [1]. Allowed spin structures in this orthoferrites are $\Gamma_1$ ($A_x$, $G_y$, $C_z$), $\Gamma_2$ ($F_x$, $C_y$, $G_z$), and $\Gamma_4$ ($G_x$, $A_y$, $F_z$), the mutual conversion of different spin configurations is known as spin reorientation. It is worth noting that the origin of SRT is not the same for different $RFeO_3$, and we generally pay attention to temperature-induced SRT. For example, $ErFeO_3$ shows an SRT from $\Gamma_4$ to $\Gamma_2$ in the temperature range between 88 K and 98 K [2], while the temperature-induced SRT disappears in $YFeO_3$ due to the filled electron shells of Y ions [1]. Not only the temperature but also magnetic field can play an inductive role for SRT. We still use $YFeO_3$ as an example; previous studies revealed that the field-driven spin reorientation occurred at a relatively high magnetic field around 7 T [3], and the dynamical SRT of $YFeO_3$ have also been studied by using terahertz spectroscopy [4].

$RFeO_3$ has two kinds of magnetic sub-lattices of $Fe^{3+}$ and $R^{3+}$, resulting in three different kinds of magnetic interactions: $Fe^{3+}$-$Fe^{3+}$, $Fe^{3+}$-$R^{3+}$ and $R^{3+}$-$R^{3+}$ interaction [1]. The $Fe^{3+}$ magnetic moments dominate magnetization at room temperature and rare-earth ions are paramagnetic. At low temperatures, rare-earth ions tend to be ordered because of the molecular field effect of $Fe^{3+}$ magnetic sub-lattices [5]. For example, $ErFeO_3$ has an antiferromagnetic structure along $a$-axis and weak ferromagnetism along $c$-axis. The $Er^{3+}$ gradually forms a magnetic moment that is opposite to the magnetic moment of $Fe^{3+}$ during the cooling process. So at a certain temperature, the overall magnetization of $ErFeO_3$ will reach zero (Zero magnetization phenomenon), which is a major mechanism for the understanding of $Er^{3+}$-$Fe^{3+}$ interaction. Similar phenomenon has also been reported in $NdFeO_3$ [6]. Another unique property of $ErFeO_3$ is that an abrupt jump of magnetization has been observed both in cooling and heating processes [7], a phenomenon called spin flip, which might lead to potential applications in developing new magnetic devices. Besides $ErFeO_3$, other $RFeO_3$ materials with the above-mentioned spin flip behaviors are: $SmFeO_3$ [8], $NdFeO_3$ [6], $Ho_{0.5}Pr_{0.5}FeO_3$ [9] and so on. Recently, there are many studies focusing on $ErFeO_3$: the magnetic structures have been investigated by neutron diffraction, corresponding symmetry and refinement [10]. Previous publications reported the giant magnetic entropy and the refrigerant capacity in the $ErFeO_3$ single crystal. The results explained the effect of $R^{3+}$-$R^{3+}$ interaction near the rare-earth ordering temperature for total magnetization [2]. Furthermore, $ErFeO_3$ has also been studied

by terahertz emission spectroscopy [11–13]. The rich magnetization behavior of $ErFeO_3$ has attracted intensive attention in the last few years. However, various interactions of $ErFeO_3$ still remain elusive.

This paper reported the study of $Er_{1-x}Y_xFeO_3$ ($x = 0$, 0.25, 0.5, 0.75, 1) single crystals. We confirm the spin reorientation between $\Gamma_4$ ($G_x$, $A_y$, $F_z$) and $\Gamma_2$ ($F_x$, $C_y$, $G_z$) and the spin flip phenomenon. By doping of nonmagnetic $Y^{3+}$, we found that the spin reorientation temperature ranges, the compensation point as well as the spin flip temperature can be tuned to low temperatures. Moreover, the structural changes are also confirmed by using Raman Spectroscopy measurement. Our study suggests that $Y^{3+}$ weakens the interaction between $Er^{3+}$ and $Fe^{3+}$ instead of introducing new magnetic structures in $ErFeO_3$.

## 2 Experimental

We have prepared a family of $Er_{1-x}Y_xFeO_3$ ($x = 0$, 0.25, 0.5, 0.75, 1) single crystals. According to stoichiometric ratio, polycrystalline samples were synthesized by conventional solid-state reaction method using $Er_2O_3$ (99.9%), $Y_2O_3$ (99.9%) and $Fe_2O_3$ (99.98%) powders. Mixtures were sintered twice for sufficient reaction at 1350 °C for 17h, and then cooled to room temperature. In the sintering process, the compounds of feed and seed rods were prepared by hydrostatic press system at 70 MPa. Single crystals were grown by optical floating zone furnace (FZ-T-10000-H-VI-P-SH, Crystal Systems Corp). During this procedure, the feed and seed rods were simultaneously rotated in opposite directions at 15 rpm, the molten zone was moved upwards at a rate of 3 mm/h. Large-size single crystals of $Er_{1-x}Y_xFeO_3$ family were obtained as shown in Fig. 1(a). The structure was characterized by X-ray diffraction (XRD, Rigaku, D/max2500) using Cu-K$\alpha$ radiation in the angle range $10° \leq 2\theta \leq 90°$. All of their crystallographic orientations were determined by back-reflection Laue X-ray photography with a tungsten target (with the X-ray beam of 0.5 mm in diameter). The Raman spectra were performed on a confocal Raman spectroscope using a 514 nm excitation laser (Renishaw, Invia Raman microscope). The Physics Property Measurement System (Quantum Design, PPMS-9) with a Vibrating Sample Magnetometer (VSM) option was used to measure the magnetization properties. We follow the Zero-field-cooling (ZFC), Field-cooled-cooling (FCC) and Field-cooled-warming (FCW) mode to measure the $M$-$T$ curves. The ZFC and FCW curves were performed during heating process and the FCC curves correspond to the cooling process.

## 3 Results and discussion

### 3.1 Structure characterization

Figures 2(a)–(e) show the powder XRD patterns of the $Er_{1-x}Y_xFeO_3$ ($x = 0$, 0.25, 0.5, 0.75, 1) family at room temperature. By using Rietveld method in the *Fullprof* program, the refinements of crystal structures are shown in Figure 2. Table 1 lists the parameters observed from

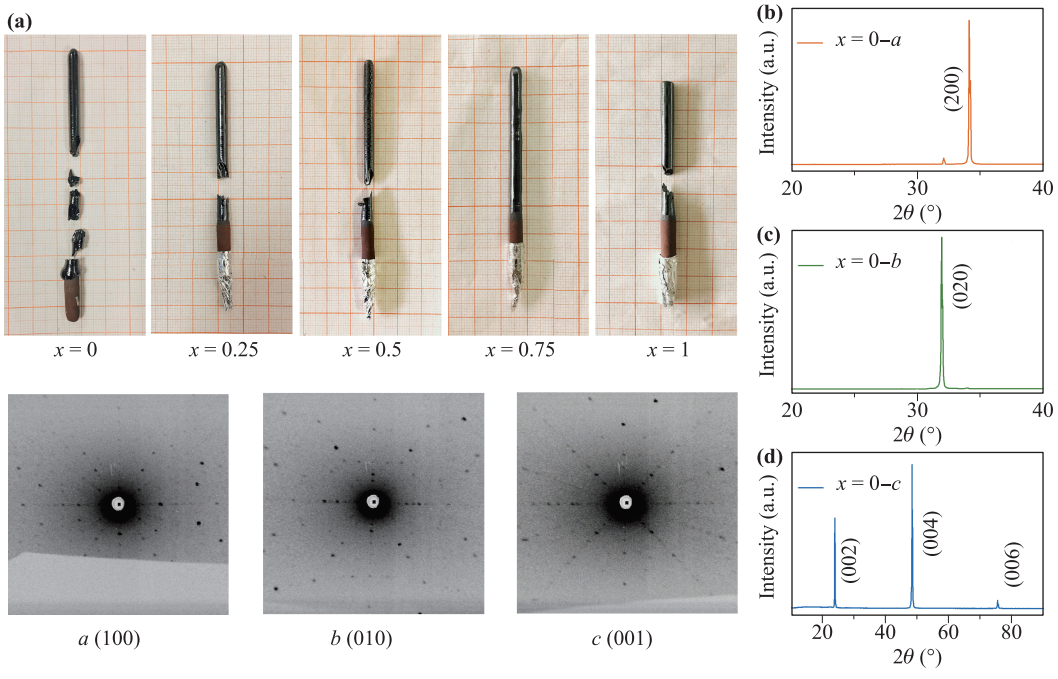


**Fig. 1** **(a)** The picture of the $Er_{1-x}Y_xFeO_3$ single crystal family and the X-ray Laue photographs of the $a$-, $b$-, and $c$-axis for $ErFeO_3$ single crystal. **(b–d)** X-ray diffraction patterns of the $ErFeO_3$ single crystal along the $a$-, $b$-, and $c$-axis, respectively.

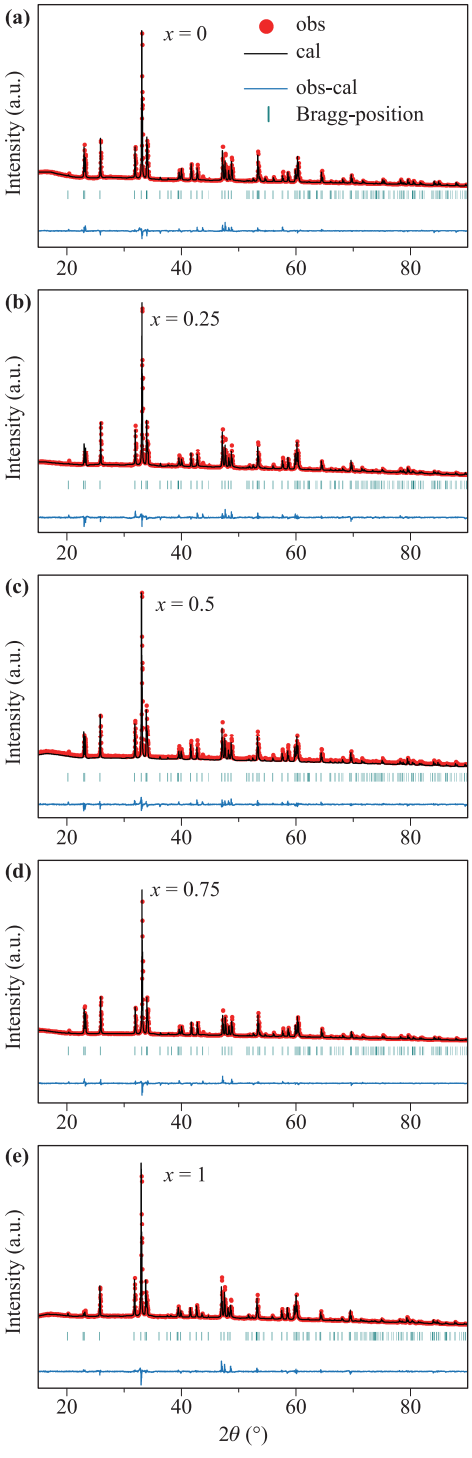


**Fig. 2** **(a–e)** Rietveld refined X-ray diffraction patterns of the $Er_{1-x}Y_xFeO_3$ single crystal family.

the Rietveld refinements for five samples. The results show that $Er_{1-x}Y_xFeO_3$ has orthorhombic perovskite structure with the space group *Pbnm* and no impurity phases are detected for all samples. Due to the small difference in ion radius, Y doping does not lead to significant changes of the crystallographic structure of $ErFeO_3$. The refinement of XRD data shows high quality of our samples.

**Table 1** Crystallographic parameters obtained from the Rietveld refinement of power XRD data of $Er_{1-x}Y_xFeO_3$.

| $Er_{1-x}Y_xFeO_3$ samples | Lattice parameters (Å) | | | Volume of crystal cell (Å$^3$) |
|---|---|---|---|---|
| | $a$ | $b$ | $c$ | |
| $x = 0$ | 5.269(3) | 5.593(4) | 7.602(0) | 224.06 |
| $x = 0.25$ | 5.271(6) | 5.593(2) | 7.604(7) | 224.23 |
| $x = 0.5$ | 5.276(7) | 5.595(2) | 7.606(9) | 224.59 |
| $x = 0.75$ | 5.281(6) | 5.598(3) | 7.608(9) | 224.98 |
| $x = 1$ | 5.285(3) | 5.601(0) | 7.613(1) | 225.38 |

Figure 1(a) presents the back-reflection Laue photograph of $ErFeO_3$ (along $a$, $b$ and $c$ axis respectively). Clear Laue spots also confirm the high quality of our samples. Moreover, Figs. 1(b)–(d) present XRD patterns along $a$, $b$, and $c$ axis, respectively. Characteristic peaks for each axis can be well indexed.

### 3.2 Raman measurements

The Raman Spectroscopy of the $RFeO_3$ compounds can provide the information of the key length, bond angle, vibration mode and other [14–18]. According to the literatures [16, 19], the irreducible representation of the center of the Brillouin district for $RFeO_3$ can be written as: $G=7A_{1g}+8A_{1u}+7B_{1g}+8B_{1u}+5B_{2g}+10B_{2u}+5B_{3g}+10B_{3u}$, which contains 24 Raman-active vibrational modes: $7A_{1g}+7B_{1g}+5B_{2g}+5B_{3g}$. In the wavenumbers range of 100-800 cm$^{-1}$, only 8-10 Raman peaks can be observed [15]. The vibration modes below 200 cm$^{-1}$ are mainly characterized by rare-earth ions, while above 300 cm$^{-1}$, they are related to the vibration of oxygen ions or $FeO_6$ octahedra. This is because the high frequency mode is mainly related to the lighter oxygen ions. Figure 3(a) shows the Raman Spectroscopy of $Er_{1-x}Y_xFeO_3$ single crystals observed at room temperature with a laser of 514 nm. Under the selected test conditions, the results show that there are five possible Raman peaks with a corresponding wave number of approximately 269 cm$^{-1}$, 342 cm$^{-1}$, 430 cm$^{-1}$, 502 cm$^{-1}$ and 643 cm$^{-1}$. According to the relevant literatures [15], we obtain the model information corresponding to the different Raman peaks, which are marked in the Figure. These peaks reflect the rotation and stretching operations associated with the oxygen ions or the $FeO_6$ octahedra. With increasing doping, minor shift of some peaks are observed. Figures 3(b) and (c) indicate the shift of Raman peaks with wave numbers around 502 cm$^{-1}$ and 430 cm$^{-1}$, respectively. The positions of two peaks vary with the doping amount of $Y^{3+}$ ions. With increasing doping, the peak near 502 cm$^{-1}$ and 430 cm$^{-1}$ are shifted to low frequency. This result is attributed to the two effects of the doped $Y^{3+}$ ions: i) the enlargement of the unit cell volume and chemical bond and ii) the reduced effective mass.

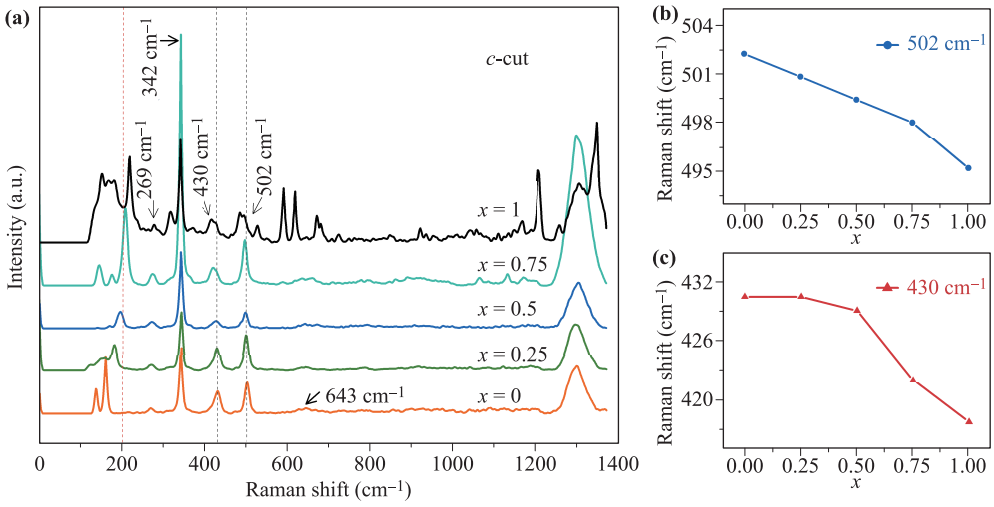


**Fig. 3** Raman spectra at room temperature of the $Er_{1-x}Y_xFeO_3$ single crystal family.

### 3.3 Magnetization measurements

The $ErFeO_3$ has been reported to show rich magnetization behaviors. In order to carefully study the effect of rare-earth ion doping on the spin reorientation phase transition and other phenomena, we choose $ErFeO_3$ as the parent phase. Figure 4(a) displays the temperature dependent magnetization ($M$-$T$) for an $ErFeO_3$ single crystal with an applied field of $H = 50$ Oe. Consistent with other results [2], the spin reorientation transition from $\Gamma_4$ ($G_x$, $A_y$, $F_z$) to $\Gamma_2$ ($F_x$, $C_y$, $G_z$) state has been observed, from $M$-$T$ curves, in the temperature range of 88 K $\leq T_{SR} \leq$ 98 K. The compensation point at $T_{comp} = 46$ K, where the magnetization goes through zero, is also observed along $a$-axis. In addition, both ZFC and FCC curves in the $a$-direction show a characteristic feature of spin flip, which appears at 66 K (for ZFC) and 26 K (for FCC). The $Y^{3+}$ only has a filled electron shell, so it does not show magnetic behaviors [13]. $Y^{3+}$ doping will not introduce new magnetic structures to $ErFeO_3$. Based on this, a family of $Er_{1-x}Y_xFeO_3$ single crystals is discussed below, the $M$-$T$ curves along $a$-axis of $Er_{1-x}Y_xFeO_3$ are shown in Fig. 5. The $M$-$T$ curves show that, with the increase of $Y^{3+}$ component in $Er_{1-x}Y_xFeO_3$, a downward trend of the spin reorientation temperature range is observed. When $x$ is increased to 1, there is no SRT in $YFeO_3$. Against the magnetization compensation phenomenon of $ErFeO_3$ we can find that, above $x = 0.75$, there is no compensation point. Comparing the ZFC and FCC curves of $a$-axis of $Er_{1-x}Y_xFeO_3$ family, it can be seen that as the doping amount of $Y^{3+}$ increases, the spin flip temperature move to low temperature.

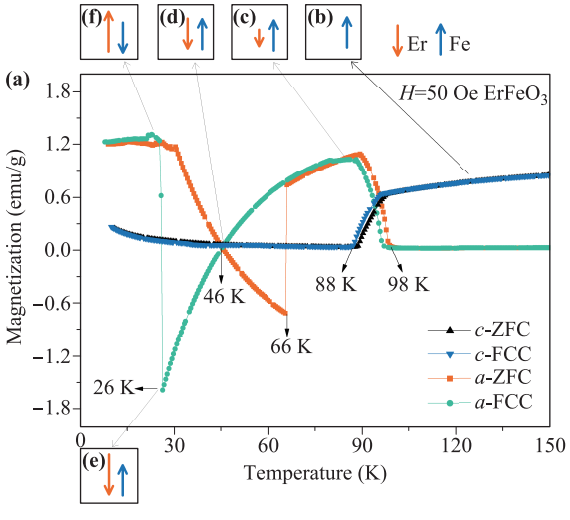


**Fig. 4** **(a)** Temperature dependence of the magnetizations of $ErFeO_3$ single crystal at $H = 50$ Oe. **(b–f)** Schematic diagram of the evolution of magnetizations arising from Er (red) and Fe (blue) ions.

Now we focus on the cooling process (FCC curves). Previous studies reported the magnetizations of Er and Fe sublattices are antiparallel to each other. Since $Y^{3+}$ is a non-magnetic ion, doping does not change the type of spin reorientation of $ErFeO_3$ but can regulate the temperature range at which this phase transition occurs. Similarly, here we mainly consider the interaction between $Er^{3+}$ and $Fe^{3+}$ at the spin flip temperature. When the temperature is much higher than the spin reorientation temperature, the overall magnetization is mainly contributed by the iron ions and the magnetic moments of $Er^{3+}$ and $Fe^{3+}$ are arranged in antiparallel direction [1]. With decreasing temperature, the contribution of the $Er^{3+}$ magnetic moment gradually increases, and then undergoes a spin reorientation transition [see Figs. 4(b)–(d)]. After this, $Fe^{3+}$ magnetic moments and $Er^{3+}$ magnetic moments (which are antiparallel to $Fe^{3+}$) compensate each other (Magnetization compensation phenomenon). When cooling the sample below 30 K, the energy of the system formed by the

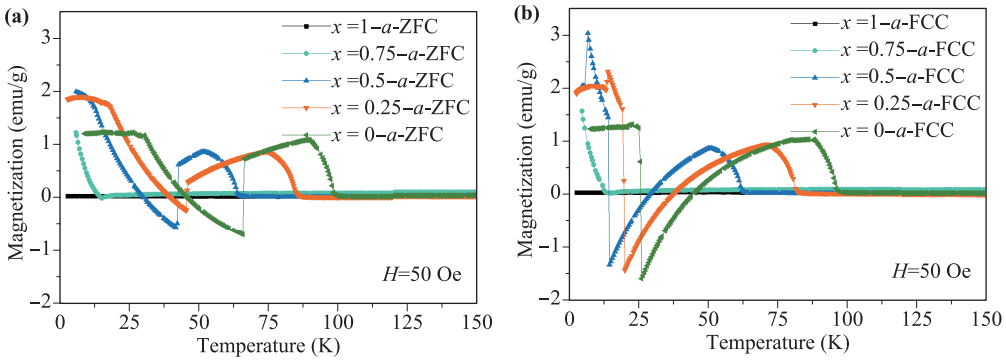


**Fig. 5** Temperature dependence of the magnetizations of the $Er_{1-x}Y_xFeO_3$ single crystals along $a$ axis.

two sublattices cannot compete with the energy of the external magnetic field, so the magnetic moments of the two sublattices are reversed together. As a result, the magnetization changes from a negative value to a positive (spin flip phenomenon) [see Figs. 4(e–f)].

The FCC curves of each sample in $Er_{1-x}Y_xFeO_3$ family are obviously inconsistent. For $x = 0.25$ and 0.5, the samples show a second magnetic jump at 14 K (for $x = 0.25$) and 7 K (for $x = 0.5$). $Y^{3+}$ does not contribute to the magnetic moment of the rare earth ion sublattice. Its addition weakens the original interaction of the system, so that the system will experience a longer period of cooling for the appearance of spin flip phenomenon. For $x = 0.75$ it is observed that the spin reorientation and the spin flip do not exist. However, there is a sharp increase in the FCC curve at 13 K. The magnetization behavior at this time is completely dominated by $Er^{3+}$ ordering. Moreover, the magnetization behavior of the heating process (ZFC curves) also presents the same phenomenon.

## 4 Conclusions

This paper focuses on the spin reorientation transition and the spin flip characteristics of $Er_{1-x}Y_xFeO_3$ family. We successfully prepared five high quality single crystals and conducted the Rietveld refinements and Raman Spectroscopy measurement to evidence the structural changes. Spectroscopy results show that there are five possible Raman peaks and some of them are shifted to low frequency with the increasing doping. By doping of nonmagnetic $Y^{3+}$, we found that the spin reorientation temperature range, the compensation point and the spin flip temperature are tuned to low temperatures. We have found that the type of spin reorientation of $ErFeO_3$ does not change in $Er_{1-x}Y_xFeO_3$ family. To summarize, $Y^{3+}$ do not introduces new magnetic structures in $ErFeO_3$ and weakens the interaction between $Er^{3+}$ and $Fe^{3+}$.

**Acknowledgements** This work was supported by the National Natural Science Foundation of China (NSFC, Grant Nos. 11774217, 51372149, and 11574194), and the Research Grant (No. 16DZ2260600) from Science and Technology Commission of Shanghai Municipality. J.-Y. G. thanks the support by The Program for Professor of Special Appointment (Eastern Scholar) at Shanghai Institutions of Higher Learning.

## References

1. L. White, Review of recent work on the magnetic and spectroscopic properties of the rare-earth orthoferrites, *J. Appl. Phys.* 40(3), 1061 (1969)
2. R. Huang, S. Cao, W. Ren, S. Zhan, B. Kang, and J. Zhang, Large rotating field entropy change in $ErFeO_3$ single crystal with angular distribution contribution, *Appl. Phys. Lett.* 103(16), 162412 (2013)
3. J. Scola, W. Noun, E. Popova, A. Fouchet, Y. Dumont, N. Keller, P. Lejay, I. Sheikin, A. Demuer, and A. Pautrat, Spin reorientation induced by a very high magnetic field in domain-structured $YFeO_3$ films: Emergence of perpendicular anisotropy, *Phys. Rev. B* 81(17), 174409 (2010)
4. X. Lin, J. Jiang, Z. Jin, D. Wang, Z. Tian, J. Han, Z. Cheng, and G. Ma, Terahertz probes of magnetic field induced spin reorientation in $YFeO_3$ single crystal, *Appl. Phys. Lett.* 106(9), 092403 (2015)
5. V. D. Buchel'nikov, N. K. Dan'shin, L. T. Tsymbal, and V. G. Shavrov, Magnetoacoustics of rare-earth orthoferrites, *Phys. Uspekhi* 39(6), 547 (1996)
6. S. J. Yuan, W. Ren, F. Hong, Y. B. Wang, J. C. Zhang, L. Bellaiche, S. X. Cao, and G. Cao, Spin switching and magnetization reversal in single-crystal $NdFeO_3$, *Phys. Rev. B* 87(18), 184405 (2013)
7. L. T. Tsymbal, Y. B. Bazaliy, G. N. Kakazei, F. Palomares, and P. E. Wigen, Magnetic hysteresis in $ErFeO_3$ near the low temperature erbium ordering transition, *Magn. IEEE Trans. On* 44(11), 2933 (2008)
8. S. Cao, H. Zhao, B. Kang, J. Zhang, and W. Ren, Temperature induced spin switching in $SmFeO_3$ single crystal, *Sci. Rep.* 4(1), 5960 (2015)
9. G. Wang, W. Zhao, Y. Cao, B. Kang, J. Zhang, W. Ren, and S. Cao, Temperature-induced spin reorientation and magnetization jump of rare-earth orthoferrite

$Ho_{0.5}Pr_{0.5}FeO_3$ single crystal, *J. Alloys Compd.* 674, 300 (2016)

10. G. Deng, P. Guo, W. Ren, S. Cao, H. E. Maynard-Casely, M. Avdeev, and G. J. McIntyre, The magnetic structures and transitions of a potential multiferroic orthoferrite Er-$FeO_3$, *J. Appl. Phys.* 117(16), 164105 (2015)
11. R. V. Mikhaylovskiy, T. J. Huisman, R. V. Pisarev, T. Rasing, and A. V. Kimel, Selective excitation of terahertz magnetic and electric dipoles in $Er^{3+}$ ions by femtosecond laser pulses in $ErFeO_3$, *Phys. Rev. Lett.* 118(1), 017205 (2017)
12. R. V. Mikhaylovskiy, E. Hendry, V. V. Kruglyak, R. V. Pisarev, T. Rasing, and A. V. Kimel, Terahertz emission spectroscopy of laser-induced spin dynamics in $TmFeO_3$ and $ErFeO_3$ Orthoferrites, *Phys. Rev. B* 90(18), 184405 (2014)
13. R. Zhou, Z. Jin, G. Li, G. Ma, Z. Cheng, and X. Wang, Terahertz magnetic field induced coherent spin precession in $YFeO_3$, *Appl. Phys. Lett.* 100(6), 061102 (2012)
14. M. K. Singh, H. M. Jang, H. C. Gupta, and R. S. Katiyar, Polarized Raman scattering and lattice eigenmodes of antiferromagnetic $NdFeO_3$, *J. Raman Spectrosc.* 39(7), 842 (2008)
15. H. C. Gupta, M. Kumar Singh, and L. M. Tiwari, Lattice dynamic investigation of Raman and infrared wavenumbers at the zone center of orthorhombic $RFeO_3$ ($R$ = Tb, Dy, Ho, Er, Tm) Perovskites, *J. Raman Spectrosc.* 33(1), 67 (2002)
16. N. Koshizuka and S. Ushioda, Inelastic-light-scattering study of magnon softening in $ErFeO_3$, *Phys. Rev. B* 22(11), 5394 (1980)
17. S. T. Zhang, Y. Zhang, M. H. Lu, C. L. Du, Y. F. Chen, Z. G. Liu, Y. Y. Zhu, N. B. Ming, and X. Q. Pan, Substitution-induced phase transition and enhanced multiferroic properties of $Bi_{1-x}La_xFeO_3$ ceramics, *Appl. Phys. Lett.* 88(16), 162901 (2006)
18. A. V. Kimel, A. Kirilyuk, A. Tsvetkov, R. V. Pisarev, and T. Rasing, Laser-induced ultrafast spin reorientation in the antiferromagnet $TmFeO_3$, *Nature* 429(6994), 850 (2004)
19. M. Udagawa, K. Kohn, N. Koshizuka, T. Tsushima, and K. Tsushima, Influence of magnetic ordering on the phonon Raman spectra in $YCrO_3$ and $GdCrO_3$, *Solid State Commun.* 16(6), 779 (1975)